Title
A Critical Role for Thermosensation in Host Seeking by Skin-Penetrating Nematodes

Journal
Current Biology, 28(14)

ISSN
0960-9822

Authors
Bryant, Astra S
Ruiz, Felicitas
Gang, Spencer S
et al.

Publication Date
2018-07-01

DOI
10.1016/j.cub.2018.05.063

Peer reviewed

HHS Public Access

Author manuscript

Curr Biol. Author manuscript; available in PMC 2019 July 23.

Published in final edited form as:

Curr Biol. 2018 July 23; 28(14): 2338–2347.e6. doi:10.1016/j.cub.2018.05.063.

A critical role for thermosensation in host seeking by skin-penetrating nematodes

Astra S. Bryant[1], **Felicitas Ruiz**[1], **Spencer S. Gang**[2], **Michelle L. Castelletto**[1], **Jacqueline B. Lopez**[1], and **Elissa A. Hallem**[1,2,3,*]

[1]Department of Microbiology, Immunology, and Molecular Genetics, University of California, Los Angeles, Los Angeles, CA 90095, USA

[2]Molecular Biology Institute, University of California, Los Angeles, Los Angeles, CA 90095, USA

Summary

Skin-penetrating parasitic nematodes infect approximately one billion people worldwide and are a major source of neglected tropical disease [1–6]. Their life cycle includes an infective third-larval (iL3) stage that searches for hosts to infect in a poorly understood process that involves both thermal and olfactory cues. Here, we investigate the temperature-driven behaviors of skin-penetrating iL3s, including the human-parasitic threadworm *Strongyloides stercoralis* and the human-parasitic hookworm *Ancylostoma ceylanicum*. We show that human-parasitic iL3s respond robustly to thermal gradients. Like the free-living nematode *Caenorhabditis elegans*, human-parasitic iL3s show both positive and negative thermotaxis, and the switch between them is regulated by recent cultivation temperature [7]. When engaging in positive thermotaxis, iL3s migrate toward temperatures approximating mammalian body temperature. Exposing iL3s to a new cultivation temperature alters the thermal switch point between positive and negative thermotaxis within hours, similar to the timescale of thermal plasticity in *C. elegans* [7]. Thermal plasticity in iL3s may enable them to optimize host finding on a diurnal temperature cycle. We show that temperature-driven responses can be dominant in multisensory contexts, such that when thermal drive is strong, iL3s preferentially engage in temperature-driven behaviors despite the presence of an attractive host odorant. Finally, targeted mutagenesis of the *S. stercoralis tax-4* homolog abolishes heat seeking, providing the first evidence that parasitic host-seeking behaviors are generated through an adaptation of sensory cascades that drive environmental navigation in *C. elegans* [7–10]. Together, our results provide insight into the behavioral strategies and molecular mechanisms that allow skin-penetrating nematodes to target humans.

*Correspondence: ehallem@ucla.edu.
[3]Lead Contact

Declaration of Interests

The authors declare no competing interests.

Author Contributions

Conceptualization, A.S.B. and E.A.H.; methodology, A.S.B. and E.A.H.; software, A.S.B.; formal analysis, A.S.B.; investigation, A.S.B., F.R., and J.B.L.; resources, A.S.B., F.R., S.S.G, and M.L.C.; writing – original draft, A.S.B. and E.A.H.; writing – review & editing, A.S.B., E.A.H., F.R., S.S.G, and M.L.C.; project administration, A.S.B. and E.A.H.; funding acquisition, E.A.H.

eTOC Blurb

Bryant *et al.* report that the infective larvae of human-parasitic skin-penetrating nematodes are highly sensitive to thermal gradients and display parasite-specific temperature-driven behaviors. The authors provide the first direct evidence that host seeking is generated through adaptations of sensory cascades conserved in free-living nematodes.

Keywords

parasitic nematodes; parasitic helminths; *Strongyloides stercoralis*; *Ancylostoma ceylanicum*; host-seeking behavior; thermotaxis; thermosensation; skin-penetrating nematodes; heat seeking

Results and Discussion

Skin-penetrating parasitic nematodes are a group of soil-transmitted helminths that includes *Strongyloides stercoralis* as well as hookworms in the genera *Ancylostoma* and *Necator* [3, 11]. In humans, chronic nematode infections primarily affect the most impoverished communities around the world, with symptoms ranging from chronic gastrointestinal distress, to stunted growth and cognitive impairment in children, to death in the case of *S. stercoralis* [1–6]. Current treatments are often insufficient, as they target ongoing infections without preventing reinfection [12]. A better understanding of how parasitic worms locate and identify suitable hosts may lead to new therapeutic strategies for preventing infections.

Skin-penetrating worms have a complex life cycle that includes multiple environmental larval stages and culminates in parasitic adulthood inside a host (Figure S1A) [13]. These worms are infective during a developmentally arrested third-larval stage (iL3) analogous to the *C. elegans* dauer stage [14–16]. iL3s are soil-dwelling and actively search for hosts using host-emitted sensory cues [13]. Skin-penetrating iL3s are only capable of using a narrow range of species as hosts [17–21]. Detection of a host animal likely involves both olfactory and thermosensory cues [13]. Early studies of thermosensation in skin-penetrating nematodes showed that the iL3s of many species respond to warmth [22–31]. However, the detailed thermosensory behaviors of parasitic nematodes require elucidation, and the molecular mechanisms that mediate thermosensation in these parasites have not yet been investigated.

Thermosensation has been extensively studied in *C. elegans*, which displays both thermotaxis navigation within their physiological temperature range (15–25°C) and active avoidance of noxious heat (>26°C) [7, 32–34]. Within their physiological range, *C. elegans* adults exhibit experience-dependent thermosensory behaviors, navigating in relation to a “remembered” cultivation temperature (T_C) [7, 34–40]. If the ambient temperature changes, the “remembered”

T_C resets to the new ambient temperature within hours [7, 34, 37, 41–43]. At temperatures in the noxious heat range, *C. elegans* adults migrate down the thermal gradient [44]. In addition, noxious heat avoidance can overcome chemical attraction, as *C. elegans* adults fail to migrate toward attractive odorants placed at temperatures above their preferred range [33].

C. elegans dauers, which are more resistant to environmental stress, are insensitive to noxious thermal stimuli that repel adults [32].

Skin-penetrating human-parasitic iL3s heat seek

To better understand the temperature-driven movement of parasitic nematodes, we first investigated the thermal preferences of two human-parasitic nematodes: *S. stercoralis* and *A. ceylanicum*. We imaged iL3 migration in precisely controlled, ethologically relevant thermal gradients using a large-format thermotaxis setup based on devices used for *C. elegans* [45] but modified for use with iL3s (Figure S1B). We found that human-parasitic iL3s display robust and sensitive heat seeking when exposed to temperatures above ambient (Video S1). When placed at 25°C, *S. stercoralis* and *A. ceylanicum* iL3s moved rapidly toward warmth in both steep (~0.53°C/cm) and shallow (0.13°C/cm) gradients (Figure 1A–B). This behavior contrasted sharply with the non-directional migration of iL3s in an isothermal environment (Figure 1A–B).

To identify the preferred temperature of human-parasitic iL3s engaged in heat seeking, we then measured the distribution of iL3s in warmer gradients that spanned human skin and core body temperatures (~31–34°C and ~37°C, respectively) [46 , 47]. *A. ceylanicum* iL3s appeared to prefer temperatures near human core body temperature (~38°C), while *S. stercoralis* preferred slightly higher temperatures (~40°C), as indicated by a decrease in directional migration at these temperatures (Figure 1C–D). A preferred temperature set higher than host skin surface temperature may create strong migratory drive toward heat sources that does not attenuate as the iL3s approach a host.

The presence of a thermal gradient affected not only directional migration of iL3s, but also their crawling speeds. iL3s in a steep thermal gradient crawled more rapidly than iL3s in a shallow thermal gradient or an isothermal environment (Figure S2A–B). Both gradient steepness and absolute temperature contributed to changes in movement speed; for example, *S. stercoralis* iL3s thermotaxing in a steep gradient ranging over cooler temperatures traveled faster than iL3s thermotaxing in an equally steep gradient ranging over warmer temperatures (Figure S2A). These results suggest that the speed at which iL3s migrate within a thermal gradient is regulated by the strength of thermal drive, consistent with similar observations in *C. elegans* [36, 44]. The rapid crawling speed of human-parasitic iL3s in steep gradients, in combination with their sensitivity to shallow gradients, indicates that thermosensation is a potent sensory cue for skin-penetrating worms.

Navigation toward host temperatures promotes local-search behavior

When we tested iL3s at temperatures above ambient and below host body temperature (T_H), thermotaxis navigation occurred on a relatively straight trajectory. In contrast, as worms approached T_H, trajectories became more curved (Figure 1A–B). We quantified this change intortuosity by calculating the distance ratio (total distance divided by maximum displacement) of individual worm tracks, where a greater distance ratio indicates a more curved trajectory. We found that iL3s in a steep thermal gradient near T_H had higher distance ratios than iL3s in a steep thermal gradient below T_H (Figure S2C–D). These results suggest

that iL3s switch from long-range navigation to local search [48, 49] as they approach T_H. In contrast to iL3s in thermal gradients below T_H, iL3s in isothermal environments below T_H showed highly curved trajectories (Figures 1A–B and S2C–D), consistent with a previous study in a different parasitic nematode [23]. The fact that iL3s engage in local search both in isothermal conditions below T_H and in thermal gradients close to T_H suggests that local search is a basal behavior inhibited by thermal drive. Thus, iL3s transition from long-range navigation to local search when thermal drive has been sufficiently diminished by proximity to T_H. Local search near T_H may function to increase the likelihood that iL3s physically contact a nearby host [24]. It may also allow iL3s to sample the environment for gustatory or olfactory cues that may provide information about whether a nearby heat source indicates the presence of a host animal.

Human-parasitic iL3s engage in positive and negative thermotaxis

In the experiments described above, iL3s were placed in thermal gradients at temperatures above ambient. Under these conditions, iL3s appeared to treat thermal cues as signaling the presence of a nearby host and displayed positive trajectories. When iL3s were instead placed near or below ambient temperature, a different mode of temperature-driven movement emerged: migration toward cooler temperatures (Figure 2A–B). For *S. stercoralis* iL3s, the switch point between positive and negative thermotaxis spanned a narrow temperature range. When iL3s were placed at 22°C, most showed negative thermotaxis (Figure 2A–C). When iL3s were placed at 23°C, the population exhibited a bimodal response such that some iL3s engaged in positive thermotaxis and others engaged in negative thermotaxis (Figure 2A–C). When placed at 25°C, nearly all of the iL3s engaged in positive thermotaxis (Figure 2A–C). Negative thermotaxis could act as a dispersal mechanism to increase the chances of finding a host. It could also function to enhance subsequent discrimination between host-emitted heat and environmental temperature gradients.

The switch between positive and negative thermotaxis is regulated by recent experience

In *C. elegans*, positive and negative thermotaxis are regulated by the T_C experienced by the worms within the past few hours [7, 34, 37, 41–43]. To test whether similar experience-dependent plasticity occurs in *S. stercoralis*, we first compared the behavior of *S. stercoralis* iL3s cultivated at 15°C for 7 days with control iL3 s that were maintained at 23°C. Whereas 23°C-cultivated iL3s displayed both positive and negative thermotaxis when placed at 23°C in a ~20–34°C gradient (Figure 2A–B), iL3s cultivated at 15°C exclusively engaged in positive thermotaxis (Figure 2D). Thus, the decision to engage in positive or negative thermotaxis depends on T_C.

To investigate the time course of the switch, we took *S. stercoralis* iL3s grown at 23°C and cultivated them at either 23°C or 15°C for 2 hours, in parallel. We then recorded their behavior after placement at 22°C in a ~20–34°C gradient. In those conditions, only a small percentage of iL3s cultivated at 23°C engaged in positive thermotaxis (Figure 2E and Video S2). iL3s cultivated for 2 hours at 15°C were significantly m ore likely to display positive thermotaxis (Figure 2E and Video S3). Conversely, iL3s cultivated for 2 hours at 37°C were

slightly less likely to engage in positive thermotaxis after placement at 30°C in a ~20–34°C gradient (Figure 2F); however, the majority of iL3s cultivated at 37°C continued to display positive thermotaxis, suggesting that thermal cues can drive host seeking even when environmental temperatures are high. Together, our results demonstrate that the time course of experience-dependent modulation in *S. stercoralis* is similar to that of T_C-dependent thermal plasticity in *C. elegans* [7, 34, 37, 41–43].

Soil-dwelling worms experience changes in environmental temperature on diurnal time scales [36, 50, 51]. Our results demonstrate that experience-dependent modulation of thermosensory responses in soil-dwelling iL3s occurs quickly enough to plausibly drive diurnal changes in host-seeking behavior. Moreover, the decrease in heat seeking we observed when T_C approximates T_H suggests that iL3s may be more likely to target humans when environmental temperatures are low. Interestingly, the rapid (hours-long) experience-dependent modulation of thermal preferences is in contrast to the slower (days-long) experience-dependent olfactory plasticity previously observed in some parasitic worms [52, 53]. Since olfactory environments are likely to be less influenced by diurnal changes than thermal environments, our results suggest that the temporal dynamics of sensory plasticity in iL3s may be tuned for the ethological relevance of environmental changes.

Similar thermotaxis behaviors are exhibited by other mammalian-parasitic nematodes

We next compared the thermal preferences of human-parasitic nematodes to those of an ethologically and evolutionarily diverse group of soil-dwelling nematodes (Figure S3A). For this analysis, we placed nematodes at 30°C in a steep thermal gradient; these conditions elicited robust positive thermotaxis from the human-parasitic iL3s (Video S1). We found that the other mammalian-parasitic species tested displayed robust positive thermotaxis under these conditions (Figure S3). Notably, we found that the passively ingested nematode *Heligmosomoides polygyrus* [54, 55] showed positive thermotaxis toward T_H (Figure S3D).

Together with previous studies showing attraction of *H. polygyrus* iL3s to host-emitted odorants [52, 55], our results suggest that at least some passively ingested iL3s host seek to position themselves near potential hosts, where they are more likely to be swallowed. As a control for these experiments, we examined the temperature-driven movement of an entomopathogenic nematode (EPN) and *C. elegans* when placed at 30°C in the same thermal gradient. A s expected [19, 21, 30], neither the EPN nor *C. elegans* adults or dauers displayed positive thermotaxis under these conditions (Figure S3E–I). Thus, movement toward T_H is limited to nematodes that infect mammalian hosts. All of the mammalian-parasitic iL3s tested also showed similar experience-dependent positive and negative thermotaxis behaviors (Figure S4), consistent with a previous study of one of these species [29].

To compare the preferred temperature of each mammalian-parasitic species, we measured iL3 distribution in gradients spanning mammalian skin and core body temperatures. The thermal preferences of species that parasitize non-human mammals were similar to those of *A. ceylanicum* iL3s; they displayed minimal positive thermotaxis near T_H (Figures 1D,

S3B–D, S3J), suggesting that their preferred temperatures approximate T_H. The behaviors of *A. ceylanicum* and the parasitic worms of non-human mammals were significantly different from those of *S. stercoralis* (Figure S3J). Thus, our data suggest that, in comparison to other mammalian-parasitic nematode species, *S. stercoralis* is particularly specialized for temperature-driven tracking of potential hosts.

Thermal drive can override attraction to host odorants

Our results indicate that temperature is a potent host cue for iL3s. Previous studies demonstrated that iL3s are also attracted to host-emitted odorants [24, 48, 52, 56, 57], raising the question of whether thermal and olfactory cues interact to regulate host seeking. Other anthropophilic organisms, such as mosquitoes, exhibit context-dependent responses to host cues, such that the presence of a potent host cue can alter the behavioral response to cues belonging to other modalities [58]. In parasitic worms, however, the interactions between different sensory modalities in the context of host attraction are not well understood.

To assess the interaction between thermosensation and chemosensation in parasitic worms, we tested the effects of a thermal gradient on the response of *S. stercoralis* iL3s to the highly attractive host odorant 3-methyl-1-butanol (also called isoamyl alcohol) [48]. When iL3s were exposed to 3m1b in an isothermal context at 27°C, t hey engaged in local search directed toward the odorant source (Figure 3A–B). In contrast, when 3m1b was placed at 27°C in a steep thermal gradient, iL3s did not engage in local search toward the 3m1b but rather displayed long-range navigation up the thermal gradient (Figure 3C–D). In the steep thermal gradient, the presence of the attractive odorant did not alter either the number of iL3s that reached the odorant source, the final temperature reached, or the tortuosity of the migratory path (Figure 3C–F). When the odorant was instead placed near host body temperature in a higher thermal gradient, the presence of the odorant both reduced the final temperature reached and increased tortuosity (Figure 3G–I), an effect that is likely due to both reduced thermal drive in the warmer gradient and increased odorant volatility. Thus, an odorant that is highly attractive in a monosensory context can be overwhelmed by the strong thermal drive experienced at temperatures below T_H.

Our results suggest that at temperatures below T_H, iL3s may prioritize temperature-driven behaviors over chemosensory responses. We cannot exclude the possibility that sufficiently potent chemosensory cues could elicit attractive responses despite strong thermal drive. Nevertheless, if thermal cues are more effective drivers of directed navigation than chemosensory cues, skin-penetrating worms may utilize a host-seeking strategy wherein iL3s track down heat sources prior to determining whether they indicate a host animal. At temperatures near T_H, olfactory or gustatory cues that are selective for their host species may then cause iL3s to engage in short-range navigation toward the host and initiate host-infection behaviors [49].

S. stercoralis tax-4 is required for positive thermotaxis

To date, no studies have directly assessed the molecular basis of thermosensation or any other sensory modality in parasitic nematodes. In contrast, the molecular basis of *C. elegans* thermosensation has been extensively studied [34, 59, 60]. To begin to elucidate the molecular mechanisms that underlie parasitic nematode thermotaxis, we asked whether the distinct temperature-driven behaviors of parasitic and free-living nematodes arise from adaptations of shared thermosensory machinery. We focused on the *tax-4* gene, since the *C. elegans tax-4* gene encodes a cyclic nucleotide-gated channel subunit that is required for thermotaxis navigation [8–10, 61]. We used *S. stercoralis* for these experiments, since *Strongyloides* species are amendable to both transgenesis and CRISPR-Cas9-mediated mutagenesis [62–65]. We first examined the expression pattern of the *S. stercoralis tax-4* homolog (*Ss-tax-4*) and found that it is expressed in multiple head neuron pairs (Figure 4A), consistent with the expression pattern of *Ce-tax-4* [8, 10, 61]. We then tested the effects of *Ss-tax-4* gene disruption on parasite heat seeking. We used CRISPR-Cas9-mediated mutagenesis to generate *S. stercoralis* iL3s in which *Ss-tax-4* expression was fully disrupted, as previously described (Figure 4B–D) [65]. Plasmids encoding Cas9, the single guide RNA, and a repair template for homology-directed repair were microinjected into *S. stercoralis* free-living adult females. The iL3 progeny from the microinjected females were individually tested in behavioral assays and then genotyped after testing.

To test the effect of *Ss-tax-4* disruption on iL3 thermotaxis, we compared the temperature-driven movements of *Ss-tax-4* iL3s to those of control iL3s generated by microinjections in which Cas9 was excluded from the injection mix (“no-Cas9 controls”). As with wild-type worms, when no-Cas9 controls were placed at 30°C and allow ed to migrate for 15 minutes, they moved rapidly up the thermal gradient (Figure 4E). In contrast, *Ss-tax-4* iL3s displayed multiple deficits in their temperature-driven behaviors (Figure 4F) such that their movements resembled those of wild-type iL3s in a room temperature isothermal context (Figure 4G). First, the movement of *Ss-tax-4* iL3s toward T_H was significantly reduced relative to that of the no-Cas9 controls (Figure 4H). Second, disruption of *Ss-tax-4* suppressed the thermal-drive-dependent inhibition of local search, resulting in distance ratios resembling those of wild-type iL3s on an isothermal plate (Figure 4I). Third, *Ss-tax-4* iL3s did not exhibit a temperature-dependent increase in crawling speed (Figure 4J). Thus, *Ss-tax-4* is required for normal iL3 thermotaxis. These results suggest that the robust heat-seeking behaviors of iL3s reflect a parasitic specialization of molecular pathways utilized for thermotaxis navigation in free-living worms.

Implications for nematode control

Soil-dwelling parasitic worms that infect humans and livestock are a major health and economic threat worldwide. Current treatments rely on periodic deworming, a strategy that has led to widespread drug resistance in livestock parasites and threatens to complicate the treatment of human patients in the near future [66–70]. Understanding the sensory modalities that guide host seeking by parasitic nematodes may enable new approaches for preventing infections. Here, we combined quantitative behavioral analyses with targeted mutagenesis to elucidate the role of thermosensation in the host-seeking behaviors of

mammalian-parasitic worms. We find evidence that heat acts as a critical host-emitted cue for multiple species of soil-transmitted helminths. Our results could inform the design of novel control strategies, such as worm traps that incorporate heating elements. Furthermore, our data suggest that parasitic nematodes modulate their response to thermal cues on a diurnal cycle such that they heat seek primarily in cooler environments. Thus, populations at risk for infection may be more susceptible to being targeted by a host-seeking nematode in the early morning and late evening, when people are active and environmental temperatures are low; this possibility has important implications for the development of preventative interventions [71]. Future studies of the cellular, molecular, and circuit bases of thermosensation in parasitic nematodes will provide further insights into the mechanisms that drive parasite-specific host-seeking behaviors.

STAR Methods

CONTACT FOR REAGENT AND RESOURCE SHARING

Further information and requests for resources and reagents should be directed to and will be fulfilled by the Lead Contact, Dr. Elissa Hallem (ehallem@ucla.edu).

EXPERIMENTAL MODEL AND SUBJECT DETAILS

All protocols and procedures involving vertebrate animals were approved by the UCLA Office of Animal Research Oversight (Protocol 2011–060–22), which adheres to the standards of the AAALAC and the *Guide for the Care and Use of Laboratory Animals.*

Maintenance of Strongyloides stercoralis—*S. stercoralis* (UPD strain) was generously provided by Dr. James Lok (University of Pennsylvania). *S. stercoralis* was serially passaged through male and female Mongolian gerbils (Charles River Laboratories) and maintained on fecal-charcoal plates as previously described [48]. Gerbils were inoculated via subcutaneous injections with ~2,250 iL3s in 200 μL of sterile PBS, under isoflurane anesthesia. To harvest fecal pellets, gerbils were housed overnight in cages with wire floors. The following morning, fecal pellets were recovered from damp cardboard below the wire floor. Feces containing *S. stercoralis* were collected for 14–45 days post-inoculation. Fecal-charcoal plates were made by mixing feces, dH_2O, and autoclaved charcoal granules (bone char from Ebonex Corp., Cat #EBO58BC.04). The mixture was poured into 10-cm-diameter Petri dishes lined with wet 10-cm-diameter Whatman filter paper. In some cases, fecal-charcoal plates were stored for ~2 days at 25°C; otherwise plates were stored for 2 days at 20°C. For microinjection, free-living males and females were collected via a Baermann apparatus [62] from plates stored at 25°C for 1 day or plates stored at 20°C for 2 days. After 2 days, all remaining plates were moved to a 23°C inc ubator until use in thermotaxis assays. For thermotaxis assays, female iL3s were retrieved from 7–14 day old fecal-charcoal plates via a Baermann apparatus. *S. stercoralis* iL3s are exclusively female. Prior to testing, iL3s were stored in BU saline [75] or water for no more than 8 hours.

Maintenance of *Ancylostoma ceylanicum*—*A. ceylanicum* (Indian strain, US National Parasite Collection Number 102954) was generously provided by Dr. John Hawdon

(George Washington University). *A. ceylanicum* was serially passaged through male Syrian golden hamsters (Envigo) and maintained on fecal-charcoal plates in a 23°C incubator as previously described [52]. Hamsters were inoculated with 70–100 iL3s in 100 μL sterile water via oral gavage. Feces containing *A. ceylanicum* were collected as described above for 14–44 days post-inoculation. Fecal-charcoal plates were made as described above and stored at 23°C until use. For thermotaxis assays, male and female *A. ceylanicum* iL3s were retrieved from 7–18 day old fecal-charcoal plates via a Baermann apparatus [62]. Prior to testing, iL3s were stored in water for no more than 8 hours.

Maintenance of *Strongyloides ratti*—*S. ratti* (ED321 strain) was generously provided by Dr. James Lok (University of Pennsylvania). *S. ratti* was serially passaged through female Sprague Dawley rats (Envigo) and maintained on fecal-charcoal plates in a 23°C incubator as previously described [48]. Rats were inoculated with 800 iL3s in 300 μL sterile PBS via subcutaneous injection. Feces containing *S. ratti* were collected as described above for 7–23 days post-inoculation. Fecal-charcoal plates were made as described above and stored at 23°C until use. For thermotaxis assays, female *S. ratti* iL3s were retrieved from 7–14 day old fecal-charcoal plates via a Baermann apparatus [62]. *S. ratti* iL3s are exclusively female. Prior to testing, iL3s were stored in water for no more than 8 hours.

Maintenance of *Nippostrongylus brasiliensis*—*N. brasiliensis* was generously provided by Dr. Edward Platzer (University of California, Riverside). *N. brasiliensis* was serially passaged through female Long Evans rats (Envigo) and maintained on fecal-charcoal plates in a 23°C incubator, as previously described [48]. Rats were inoculated with ~4,000 iL3s in 300 μL sterile PBS via subcutaneous injection. Feces containing *N. brasiliensis* were collected as described above for 6–9 days post-inoculation. Fecal-charcoal plates were made as above and stored at 23°C until use. For thermotaxis assays, male and female *N. brasiliensis* iL3s were retrieved from 7–14 day old fecal-charcoal plates via a Baermann apparatus [62]. Prior to testing, iL3s were stored in water for no more than 8 hours.

Maintenance of *Heligmosomoides polygyrus*—*H. polygyrus* was generously provided by Dr. Raffi Aroian (University of Massachusetts Medical School). *H. polygyrus* was serially passaged in male and female C57BL/6 mice (UCLA Division of Laboratory Animal Medicine Breeding Colony or Jackson Labs) and maintained on fecal-charcoal plates at room temperature, as previously described [52]. Mice were inoculated with 100–150 iL3s in 100 μL sterile water via oral gavage. Feces containing *H. polygyrus* were collected as described above for 10–65 days post-inoculation. Fecal-charcoal plates were made as described above and stored at room temperature (21–23°C) until use. For thermotaxis assays, male and female *H. polygyrus* iL3s were retrieved from 7–14 day old fecal-charcoal plates via a Baermann apparatus [62]. Prior to testing, iL3s were stored in water for no more than 8 hours.

Maintenance of *Steinernema carpocapsae*—*S. carpocapsae* (ALL strain) was maintained via passage through waxworms, as previously described [53]. 3–6 last instar *Galleria mellonella* larvae were place in a 5-cm Petri dish lined with 55-mm Whatman 1 filter paper. Approximately 250 μL of dH_2O containing 1000–2000 infective juveniles (IJs)

was placed directly on the waxworms and on the filter paper. At 9 days post-exposure, infected waxworms were placed in White traps [76]; male and female IJs were collected from the White traps after 3–5 days. IJs were suspended in 10 mL ddH_2O in 50 mL tissue culture flasks and used for thermotaxis assays and to start new infections. Infection and storage of IJs was at room temperature. For thermotaxis assays, male and female IJs were used within 7 days of collection from White traps.

Maintenance of *C. elegans*—The California (CB4858) strain of *C. elegans* was used exclusively for this study. Experiments were carried out on young adult hermaphrodites and dauer larvae. To match cultivation conditions between *C. elegans* and the parasitic nematodes, *C. elegans* were maintained in the same 23°C incubator as the parasitic nematodes. Adults were raised on 2% Nematode Growth Media (NGM) plates containing a thin lawn of *Escherichia coli* OP50 bacteria, as per standard methods [77]. Adults were collected by washing them off of plates and into M9 solution [77] immediately prior to the assay. Suspended worms were collected in a watch glass; excess OP50 was rinsed off and worms were allowed to gravity settle. Dauers were generated from starved cultures [78]. In brief, ~5 L4 larvae or young adults were transferred to a fresh 2% NGM plate containing OP50. After approximately 10 days, dauers were collected from water droplets placed on the lid. Dauer formation plates were stored in the 23°C incubator, which significantly improved the rate of dauer formation. Dauer morphology was visually confirmed prior to thermotaxis experiments, and dauers were used for experiments within 7 days of their appearance on a plate.

METHOD DETAILS

Thermotaxis assays—Thermotaxis assays were performed using a large-format linear thermal stage adapted from those previously described [45]. A thermal gradient was established across an anodized aluminum slab (24x12x1/4 inch) that stands on two aluminum reservoir blocks (4x12x1.5 inch). Each reservoir block is attached to two 200-W thermoelectric heating/cooling devices (TECs, MCTE1-19913L-S, Multicomp), which transfer heat/cold between the reservoir block and commercial water blocks (MCW820, Swiftech) attached to a temperature-controlled recirculating antifreeze coolant bath (5150 R28, Fisher Scientific). The outputs of the “hot” and “cold” side thermoelectric devices are controlled by independent closed-loop circuits that each include: a thermistor attached to the aluminum slab near the “hot” or “cold” edge of the gradient (#6568T46, McMaster Carr), a PID controller (FTC100D, Accuthermo Technology) and H-bridge amplifier (FTX300, Accuthermo Technology), and a 12V switching power supply (S-320-12, Oven Industries). The temperature range is set using FTC100D software (Accuthermo Technology). A square plastic dish (22x22 cm, Corning Bioassay Dishes, Fisher Scientific) filled with 3% thermotaxis agar solution (3% w/v agar, 51.37 mM NaCl; 1 mM $CaCl_2$; 1 mM $MgSO_4$; and 5 mM KPO_4) [45] was placed in the center of the aluminum slab, with glycerol between the dish and the aluminum surface to ensure strong thermal transfer. The size of the agar surface available for worm migration was empirically measured at ~22.5 x 22.5 cm; this value was used to calculate gradient steepness. Surrounding the agar plate, an array of red LED strips provided dark-field illumination. Isothermal assays were performed using the same setup, except that a thermal gradient was not applied. For isothermal room temperature (RT)

assays, “room temperature” was between 21°C and 23°C. For all isothermal assays, the surface temperature of individual isothermal plates varied by less than 1°C and any temperature variations were not directional.

Prior to the start of an experiment, the temperature range on the agar surface was manually confirmed using a laser thermometer. Worms were deposited on the agar surface in ~3 μL of BU saline (for *S. stercoralis*) [75], M9 solution (for *C. elegans*) [77], or dH_2O (for all other species). Worm movements were monitored using two 5 mega-pixel CMOS cameras (BTE-B050-U, Mightex Systems) equipped with zoom lenses (LMZ69M, Kowa). Each camera records approximately half of the 22-cm-long thermal plate. Image acquisition was triggered using a custom MATLAB script (MathWorks) that generated precisely timed TTL pulses via a USB DAQ device (U3-LV, LabJack Corp). The TTL pulses were passed to both cameras, which in turn sent acquired images to image acquisition software (see below).

Behavioral effects of cultivation temperature—For testing the effect of long-term cultivation temperature changes in iL3 behavior, 7-day-old fecal-charcoal plates were stored for an additional 7 days at either 15°C or 23°C. iL3s were collected using a Baermann apparatus [62] and stored in a watch glass containing BU saline [75] or dH_2O at their cultivation temperature. For testing the effect of short-term cultivation temperature changes, *S. stercoralis* iL3s were collected and placed in a watch glass containing BU saline [75]. Some worms were used immediately to generate the zero timepoint. The remaining worms were divided into two watch glasses; one watch glass was placed in an incubator set to 23°C, the other was placed in an incubator set to 15°C or 37°C. After 2 hours, iL3s were assayed using the thermotaxis setup described above.

Thermotaxis assay data analysis—The population-level movement of worms in a thermal gradient was calculated using Fiji [79]. Images corresponding to the desired experimental time point were divided into 1°C bins using the Grid command, and the number of worms in each bin was tallied using the Cell Counter plug-in. A Wacom tablet and stylus (CTH-690AK, Wacom Intuos Art) were used to aid the quantification of worm location. The percent of heat-seeking worms was calculated in Excel as the sum of worms found in temperature bins above T_{start} divided by the total number of worms.

The percent of cold-seeking worms was calculated as the sum of worms found in temperatures below T_{start} divided by the total number of worms. The percent of “non-responding” worms was calculated as the number of worms that did not leave the 1°C T_{start} bin divided by the total number of worms.

For tracking individual iL3 trajectories, either single or a small group (<100) of iL3s were placed on a thermotaxis plate and their migration imaged for 10–15 minutes at a rate of 0.5 frames/second. Worm locations were measured *post-hoc* using the Manual Tracking plugin for Fiji. Custom MATLAB scripts (available upon request) were used to translate pixel-based x/y coordinates into cm- and temperature-based coordinates, which were then plotted. These scripts also calculated: overall mean speed, mean speed within specified temperature bins, distance ratio (maximum distance traveled divided by the maximum displacement), and final temperature difference (final temperature minus starting temperature).

Multisensory assays—For measuring the effect of a host odorant on the migration of individual iL3s, in both thermal gradients and isothermal conditions, 5μL undiluted 3-methyl-1-butanol was placed on the thermotaxis plate immediately prior to placement of iL3s. The effect of 3m1b was quantified by counting the number of iL3s that entered a 2 cm-diameter scoring region surrounding the odorant droplet. Only iL3s that entered the scoring region within the first 5 minutes of the assay were counted. Control (−3m1b) values were generated by counting the number of iL3s that entered a similarly positioned scoring region on a plate without odorant.

Generation of the *Strongyloides tax-4p::GFP* reporter construct—The *S. ratti tax-4* gene (SRAE_2000234000) was identified based on sequence homology with *C. elegans tax-4* and was predicted in WormBase Parasite as an ortholog of *Ce-tax-4* [72, 73]. To generate the *Sr-tax-4p::GFP* construct, ~2,100 base pairs of the *Sr-tax-4* promoter upstream of the predicted *Sr-tax-4* ATG was PCR-amplified and cloned into the *Strongyloides* expression vector pPV254 (containing *Ss-act-2p::GFP*; a gift from Dr. James Lok) in place of the *Ss-act-2* promoter. Primer sequences are listed in Table S1. To generate *Sr-tax-4p::GFP*-expressing transgenics, the plasmid encoding *Sr-tax-4p::GFP* (pMC41) was microinjected at 50 ng/μL.

CRISPR-Cas9-mediated targeted mutagenesis of *Ss-tax-4*—The *S. stercoralis tax-4* gene (SSTP_0000981000) was previously targeted for CRISPR-Cas9-mediated mutagenesis [65]; we utilized the same CRISPR target site in this study. In brief, the *Ss-tax-4* gene was identified based on sequence homology with *C. elegans tax-4* and was also predicted in WormBase Parasite as an ortholog of *Ce-tax-4* [65, 72, 73]. The CRISPR target site was identified using the Find CRISPR Site plugin for the Geneious 9 software [80]. Gene-structure diagrams for *S. stercoralis and C. elegans* were generated with Exon-Intron Graphic Maker (Version 4, www.wormweb.org). The single guide RNA (sgRNA) expression vector for targeting *Ss-tax-4* (pMC47) was synthesized by GENEWIZ and included 500- and 277-bp regions of the *S. ratti* U6 promoter and 3'UTR, respectively. The target sequence for *Ss-tax-4* is listed in the Key Resources Table. To generate the repair template (pEY11), 539-bp 5' and 671-bp 3' homology arms flanking *Ss-tax-4* site #1 were cloned into the *Strongyloides act-2p::mRFPmars* expression vector pAJ50 (a gift from Dr. James Lok). The *act-2* gene encodes actin; the *act-2* promoter drives expression of mRFPmars in body-wall muscle [74]. pEY11 was modified from pEY09 [65] to maximize targeting efficiency and improve homology-directed repair at *Ss-tax-4*.

Primer sequences are listed in the Key Resources Table and Table S1. Injection mixes contained 60 ng/μL pMC47, 20 ng/μL pEY11, and 20 ng/μL pPV540 (*Strongyloides*-codon-optimized *Cas9* driven by the *S. ratti eef-1A* promoter; a gift from Dr. James Lok). For generating no-Cas9 controls, injection mixes contained only 60 ng/μL pMC47 and 20 ng/μL pEY11. Plasmid vectors were diluted to the desired concentration in ddH_2O and filtered using a bench-top centrifuge and a 0.22-μm tube filter (Costar Spin-X, Cat #8106).

Microinjection of *Strongyloides* free-living adults—Plasmid vectors were injected into the syncytial gonad of *S. stercoralis* free-living adult females as previously described [65, 74]. For CRISPR/Cas9-mediated mutagenesis, a repair template containing

act-2p::mRFPmars was included to enable selection of transgenic F_1 progeny, as described above. In addition, the *Ss-tax-4* iL3s tested were generated from multiple injection runs. For all microinjection experiments, microinjected females were placed with wild-type adult males on fecal-charcoal plates containing uninfected gerbil feces for a minimum of 6 days prior to testing.

Selection of F_1 *Ss-tax-4* iL3s—F_1 iL3 progeny of microinjected females were recovered using a Baermann apparatus [62], washed three times in dH_2O, and then collected in BU saline [75]. ~15 μL of F_1 iL3-containing BU saline was placed on an OP50-seeded 2% NGM plate and screened for *mRFPmars* expression using a Leica M165 FC microscope. Previous studies have found that near-uniform *mRFPmars* expression in the body wall is predictive of successful homology-directed repair [65]. In contrast, sparse *mRFPmars* expression correlates with extrachromosomal-array-mediated expression. Thus, only iL3s displaying near-uniform *mRFPmars* expression were picked into a small watch glass containing BU saline; a percentage of these worms were expected to show either deletions or integration of the repair template at the target region [65]. *mRFPmars*-expressing iL3s were tested in thermotaxis assays within 8 hours of screening.

***Ss-tax-4* thermotaxis assays—**Single *mRFPmars*-expressing *S. stercoralis* iL3s were placed at 30°C in a 20–34°C thermal gradient and allowed to navigate for up to 15 minutes. Worm movements were imaged at 0.5 frames/second using the image acquisition setup described above. Image acquisition lasted for 15 minutes, until the iL3 reached the edge of the gradient, or until it left the cameras' fields of view, whichever came first. Following the cessation of recording, single iL3s were recollected for individual genomic DNA preparations. Individual iL3 trajectories were tracked as described above. Thus, all behavioral assays were performed by a researcher blind to the iL3 genotype.

Genotyping for *Ss-tax-4* gene disruptions—*mRFPmars*-positive iL3s in which *Ss-tax-4* expression was fully disrupted either by deletion or integration events (hereafter called *Ss-tax-4* iL3s) were identified by *post-hoc* single-worm genotyping, as previously described [65]. After completion of thermotaxis assays, iL3s were transferred from thermotaxis plates into PCR tubes containing 5 μL of nematode lysis buffer (50 mM KCl, 10 mM Tris pH 8, 2.5 mM $MgCl_2$, 0.45% Nonidet-P40, 0.45% Tween-20, 0.01% gelatin in ddH_2O, ~0.12 μg/μL Proteinase-K, and ~1.7% 2-mercaptoethanol). Tubes were placed at −80°C for a minimum of 20 minutes, then digested in a thermocycler (65°C (2 h), 95°C (15 min), 10°C (hold)). Digested single-iL3 DNA samples were stored at −20°C until use, for no more than 12 hours. Single DNA preparations were divided between four PCR reactions: a control reaction that amplified part of the endogenous *Ss-act-2* gene, a reaction that amplified only wild-type *tax-4,* and reactions for 5' and 3' integration of repair template pEY11 into the *Ss-tax-4* targeting site. Primer sequences are listed in the Key Resources Table. All PCR reactions were performed with GoTaq G2 Flexi DNA Polymerase (Promega, Cat #M7801) using the following thermocycler conditions: denature 95°C (2 min); PCR 95°C (30 s), 55°C (30 s), 72°C (2 min) x 35 cycles; final extension 72°C (5 min); 10°C (hold). PCR products were resolved on ~1 % agarose gels treated with GelRed (Biotium, Cat #41003) using a 1-kb ladder (NEB, Cat #N3232L). For all samples, 30 μL of PCR product were loaded on the gel,

and all samples from a single iL3 were run on the same gel. The strength of the *Ss-tax-4* wild-type band in *Ss-tax-4* worms was calculated relative to that of a wild-type iL3. Quantification was performed using a ChemiDoc MP Imaging System. Worms were categorized as *Ss-tax-4* if the Image Lab Version 5.1 Relative Quantity Tool failed to detect a wild-type *tax-4* amplification band. Some *Ss-tax-4* iL3s had either 5' or 3' integration bands, reflecting integration of pEY11; other iL3s lacked wild-type and integration bands, likely indicating a large deletion at the *Ss-tax-4* target site, as previously observed [65].

Fluorescent microscopy—Images of animals expressing *Sr-tax-4::GFP* were acquired as previously described [65]. F_1 L2-L3 larvae on a 2% NGM plate with OP50 were screened for GFP expression using a Leica M165 FC microscope. L2-L3s expressing *GFP* were exposed to 10 mM levamisole in BU saline [75], and then mounted on a slide with 5% Noble agar dissolved in ddH_2O. Epifluorescence and DIC images were taken using a Zeiss AxioImager A2 microscope with an attached Zeiss Axiocam camera. Images were processed using the Zeiss AxioVision software. Image montages were generated using Fiji [79].

QUANTIFICATION AND STATISTICAL ANALYSIS

Statistical analyses and power analyses to determine appropriate sample sizes were conducted using GraphPad Prism 6. When one-way and two-way ANOVAs are utilized, we report multiplicity-adjusted *p* values. K-means clustering was performed using PAST 3.19 [81].

KEY RESOURCES TABLE

REAGENT or RESOURCE	SOURCE	IDENTIFIER
Bacterial and Virus Strains		
Escherichia coli: Strain OP50	*Caenorhabditis* Genetics Center	OP50
Experimental Models: Organisms/Strains		
Caenorhabditis elegans: Strain CB48558	*Caenorhabditis* Genetics Center	*C. elegans* California wild isolate
Strongyloides stercoralis: UPD Strain	Dr. James Lok	*S. stercoralis*
Ancylostoma ceylanicum: Indian Strain	US National Parasite Collection Number 102954, courtesy of Dr. John Hawdon	*A. ceylanicum*
Strongyloides ratti: ED321 strain	Dr. James Lok	*S. ratti*
Nippostrongylus brasiliensis	Dr. Edward Platzer	*N. brasiliensis*
Heligmosomoides polygyrus	Dr. Raffi Aroian	*H. polygyrus*
Steinernema carpocapsae: ALL strain	[33]	*S. carpocapsae*
Meriones unguiculatus: Mongolian	Charles River Laboratories	Gerbils
Mesocricetus auratus: Syrian Golden	Envigo	Hamsters
Rattus norvegicus: Sprague Dawley	Envigo	Rats
Rattus norvegicus: Long Evans	Envigo	Rats
Mus musculus: C57BL/6	UCLA Division of Laboratory Animal Medicine Breeding Colony; Jackson Labs	Mice
Galleria mellonella larvae	Petco; American Cricket Ranch	Waxworms
Chemicals, Peptides, and Recombinant Proteins		
Charcoal granules (bone char)	Ebonex Corp.	Cat #EBO58BC.04
Oligonucleotides		
GTAACATTTGACTTGATGGGTGG	[48]	*Ss-tax-4* CRISPR target sequence

REAGENT or RESOURCE	SOURCE	IDENTIFIER
See Table S1 for primer sequences.		
Recombinant DNA		
Sr-eef-1A$_{pro}$*::Cas9::Ss-era-1* 3'UTR	Dr. James Lok; [48]	pPV540; *Strongyloides* codon-optimized Cas9
Sr-U6$_{pro}$*::Ss-tax-4-sgRNA-1::Sr-U6* 3'UTR	[48]	pMLC47; sgRNA for *Ss-tax-4*
5'HA::*Ss-act-2*$_{pro}$*::mRFPmars::Ss-era-1* 3'UTR::3'HA	This paper	pEY11; HDR construct for *Ss- tax-4*
Sr-tax-4$_{pro}$*::GFP:: Ss-era-1* 3'UTR	This paper	pMC41
Software and Algorithms		
GraphPad Prism 6	GraphPad	http://ww.graphpad.com
Zeiss AxioVision 4.8	Carl Zeiss	https://www.zeiss.com/microscopy/us/products/microscope-software/axiovision.html
Fiji	[61]	https://fiji.sc/
PAST 3.19	[62]	https://folk.uio.no/ohammer/past/
MATLAB R2107B	MathWorks	https://www.mathworks.com/products/matlab.html
Mightex Cam Demo v1.2.1	Mightex Systems	http://www.mightexsystems.com/
FTC100D TEC controller	Accuthermo Technology	http://www.accuthermo.com/
Other		
3% thermotaxis agar (17 g agar, 3 g NaCl, 1 mL 1M $CaCl_2$, 1 mL 1M $MgSO_4$, 25 mL 1M KH_2PO_4 pH 6.0, dH_2O to 1 L)	[17]	Thermotaxis agar
M9 solution (3 g KH_2PO_4, 6 g Na_2HPO_4, 5 g NaCl, 1 mL 1 M $MgSO_4$, dH_2O to 1 L)	[59]	M9 solution
BU saline (7.10 g Na_2HPO_4, 2.99 g KH_2PO_4, 4.09 g NaCl, dH_2O to 1 L)	[57]	BU saline
2% NGM plates (3 g NaCl, 2.5 g Bacto Peptone, 20 g agar, 1 mL 5mg/mL cholesterol, 1 mL 1M $CaCl_2$, 1 mL 1M $MgSO_4$, 25 mL 1M KPO_4 pH 6.0, dH_2O to 1 L)	[59]	2% NGM plates
USB-DAQ device	LabJack Corp	U3-LV
Isotemp Refrigerated/Heated Water Bath	Fisher Scientific	13-874-126
Commercial water block	Swiftech	MCW820
5-megapixel CMOS camera	Mightex Systems	BTE-B050-U
Zoom lenses	Kowa America Corp	LMZ69M
H-bridge amplifier	Accuthermo Technology	FTX300
TEC temperature controller	Accuthermo Technology	FTC100D
Peltier element	Multicomp	MCTE1-19913L-S
22x22 cm Bioassay dishes	Corning	431301
Wacom Intuos Art touch tablet and stylus	Wacom	CTH-690AK

Supplementary Material

Refer to Web version on PubMed Central for supplementary material.

Acknowledgments

We thank Josh Hawk and Joon Ha Lee (Daniel Colon-Ramós lab) for helpful discussion regarding *C. elegans* thermotaxis as well as invaluable technical advice, Navonil Banerjee for insightful comments on the manuscript, and Tiffany Mao and Emily Yang for technical assistance. This work was supported by an A.P. Giannini Postdoctoral Fellowship and NIH Ruth L. Kirschstein National Research Service Award T32NS058280 (A.S.B.); the Whitcome Predoctoral Training Program, UCLA Molecular Biology Institute, and Ruth L. Kirschstein National Research Service Award T32AI007323 (S.S.G.); the UCLA-Howard Hughes Medical Institute Pathways to Success Program (J.B.L.); and a Burroughs-Wellcome Fund Investigators in the Pathogenesis of Disease Award, NIH New Innovator Award 1DP2DC014596, and Howard Hughes Medical Institute Faculty Scholar Award (E.A.H.).

References

1. Bethony J, Brooker S, Albonico M, Geiger SM, Loukas A, Diemert D, Hotez PJ. Soil-transmitted helminth infections: ascariasis, trichuriasis, and hookworm. Lancet. 2006; 367:1521–1532. [PubMed: 16679166]
2. Schafer TW, Skopic A. Parasites of the small intestine. Curr Gastroenterol Rep. 2006; 8:312–320. [PubMed: 16836943]
3. Bisoffi Z, Buonfrate D, Montresor A, Requena-Mendez A, Munoz J, Krolewiecki AJ, Gotuzzo E, Mena MA, Chiodini PL, Anselmi M, et al. *Strongyloides stercoralis*: a plea for action. PLoS Negl Trop Dis. 2013; 7:e2214. [PubMed: 23675546]
4. Buonfrate D, Requena-Mendez A, Angheben A, Munoz J, Gobbi F, Van Den Ende J, Bisoffi Z. Severe strongyloidiasis: a systematic review of case reports. BMC Infect Dis. 2013; 13:78. [PubMed: 23394259]
5. Nutman TB. Human infection with *Strongyloides stercoralis* and other related *Strongyloides* species. Parasitology. 2016:1–11.
6. McKenna ML, McAtee S, Bryan PE, Jeun R, Ward T, Kraus J, Bottazzi ME, Hotez PJ, Flowers CC, Mejia R. Human intestinal parasite burden and poor sanitation in rural Alabama. Am J Trop Med Hyg. 2017; 97:1623–1628. [PubMed: 29016326]
7. Hedgecock EM, Russell RL. Normal and mutant thermotaxis in the nematode *Caenorhabditis elegans*. Proc Natl Acad Sci USA. 1975; 72:4061–4065. [PubMed: 1060088]
8. Komatsu H, Mori I, Rhee JS, Akaike N, Ohshima Y. Mutations in a cyclic nucleotide-gated channel lead to abnormal thermosensation and chemosensation in *C. elegans*. Neuron. 1996; 17:707–718. [PubMed: 8893027]
9. Komatsu H, Jin YH, L'Etoile N, Mori I, Bargmann CI, Akaike N, Ohshima Y. Functional reconstitution of a heteromeric cyclic nucleotide-gated channel of *Caenorhabditis elegans* in cultured cells. Brain Res. 1999; 821:160–168. [PubMed: 10064800]
10. Coburn CM, Bargmann CI. A putative cyclic nucleotide-gated channel is required for sensory development and function in *C. elegans*. Neuron. 1996; 17:695–706. [PubMed: 8893026]
11. Prichard RK, Basanez MG, Boatin BA, McCarthy JS, Garcia HH, Yang GJ, Sripa B, Lustigman S. A research agenda for helminth diseases of humans: intervention for control and elimination. PLoS Negl Trop Dis. 2012; 6:e1549. [PubMed: 22545163]
12. Jia TW, Melville S, Utzinger J, King CH, Zhou XN. Soil-transmitted helminth reinfection after drug treatment: a systematic review and meta-analysis. PLoS Negl Trop Dis. 2012; 6:e1621. [PubMed: 22590656]
13. Gang SS, Hallem EA. Mechanisms of host seeking by parasitic nematodes. Mol Biochem Parasitol. 2016; 208:23–32. [PubMed: 27211240]
14. Viney ME, Thompson FJ, Crook M. TGF-β and the evolution of nematode parasitism. Int J Parasitol. 2005; 35:1473–1475. [PubMed: 16139836]
15. Crook M. The dauer hypothesis and the evolution of parasitism: 20 years on and still going strong. Int J Parasitol. 2014; 44:1–8. [PubMed: 24095839]
16. Hotez P, Hawdon J, Schad GA. Hookworm larval infectivity, arrest and amphiparatenesis: the *Caenorhabditis elegans* Daf-c paradigm. Parasitol Today. 1993; 9:23–26. [PubMed: 15463660]
17. Haley AJ. Biology of the rat nematode *Nippostrongylus brasiliensis* (Travassos, 1914). I. Systematics, hosts and geographic distribution. J Parasitol. 1961; 47:727–732. [PubMed: 13903817]
18. Viney M, Kikuchi T. *Strongyloides ratti* and *S. venezuelensis* - rodent models of *Strongyloides* infection. Parasitology. 2017; 144:285–294. [PubMed: 26935155]
19. Bezubik B. Failure to establish infection in rats and guinea pigs exposed to the larvae of *Strongyloides papillosus*. Acta Parasitol. 1965; 13:349–354.
20. Nolan TJ, Zhu X, Ketschek A, Cole J, Grant W, Lok JB, Schad GA. The sugar glider (*Petaurus breviceps*): a laboratory host for the nematode *Parastrongyloides trichosuri*. J Parasitol. 2007; 93:1084–1089. [PubMed: 18163342]

21. Viney ME, Lok JB. The biology of *Strongyloides spp*; WormBook. 2015. 1–17. www.wormbook.org
22. Barrett J. The effect of temperature on the development and survival of the infective larvae of *Strongyloides ratti* Sandground, 1925. Parasitology. 1968; 58:641–651. [PubMed: 5740547]
23. Croll NA, Smith JM. Mechanism of thermopositive behavior in larval hookworms. J Parasitol. 1972; 58:891–896. [PubMed: 4637624]
24. Granzer M, Hass W. Host-finding and host recognition of infective *Ancylostoma caninum* larvae. Int J Parasitol. 1991; 21:429–440. [PubMed: 1917283]
25. Gupta SP. Mode of infection and biology of infective larvae of *Molineus barbatus* Chandler, 1942. Exp Parasitol. 1963; 13:252–255. [PubMed: 13951325]
26. Haas W, Haberl B, Idris SI, Kersten S. Infective larvae of the human hookworms *Necator americanus* and *Ancylostoma duodenale* differ in their orientation behaviour when crawling on surfaces. Parasitol Res. 2005; 95:25–29. [PubMed: 15614586]
27. Parker JC, Haley AJ. Phototactic and thermotactic responses of the filariform larvae of the rat nematode *Nippostrongylus muris*. Exp Parasitol. 1960; 9:92–97. [PubMed: 14430498]
28. Reesal MR. Observations on the biology of the infective larvae of *Strongyloides agoutii*. Can J Zool. 1951; 29:109–115.
29. Tobata-Kudo H, Shimada M, Koga M, Tada I. *Strongyloides ratti*: thermokinetic behavior of third-stage larvae on a temperature gradient. Exp Parasitol. 2000; 95:196–201. [PubMed: 10964647]
30. Bhopale VM, Kupprion EK, Ashton FT, Boston R, Schad GA. *Ancylostoma caninum*: the finger cell neurons mediate thermotactic behavior by infective larvae of the dog hookworm. Exp Parasitol. 2001; 97:70–76. [PubMed: 11281703]
31. Lopez PM, Boston R, Ashton FT, Schad GA. The neurons of class ALD mediate thermotaxis in the parasitic nematode, *Strongyloides stercoralis*. Int J Parasitol. 2000; 30:1115–1121. [PubMed: 10996330]
32. Wittenburg N, Baumeister R. Thermal avoidance in *Caenorhabditis elegans*: an approach to the study of nociception. Proc Natl Acad Sci USA. 1999; 96:10477–10482. [PubMed: 10468634]
33. Glauser DA, Chen WC, Agin R, Macinnis BL, Hellman AB, Garrity PA, Tan MW, Goodman MB. Heat avoidance is regulated by transient receptor potential (TRP) channels and a neuropeptide signaling pathway in *Caenorhabditis elegans*. Genetics. 2011; 188:91–103. [PubMed: 21368276]
34. Garrity PA, Goodman MB, Samuel AD, Sengupta P. Running hot and cold: behavioral strategies, neural circuits, and the molecular machinery for thermotaxis in *C. elegans* and *Drosophila*. Genes Dev. 2010; 24:2365–2382. [PubMed: 21041406]
35. Ito H, Inada H, Mori I. Quantitative analysis of thermotaxis in the nematode *Caenorhabditis elegans*. J Neurosci Methods. 2006; 154:45–52. [PubMed: 16417923]
36. Ramot D, MacInnis BL, Lee HC, Goodman MB. Thermotaxis is a robust mechanism for thermoregulation in *Caenorhabditis elegans* nematodes. J Neurosci. 2008; 28:12546–12557. [PubMed: 19020047]
37. Clark DA, Gabel CV, Lee TM, Samuel AD. Short-term adaptation and temporal processing in the cryophilic response of *Caenorhabditis elegans*. J Neurophysiol. 2007; 97:1903–1910. [PubMed: 17151225]
38. Jurado P, Kodama E, Tanizawa Y, Mori I. Distinct thermal migration behaviors in response to different thermal gradients in *Caenorhabditis elegans*. Genes Brain Behav. 2010; 9:120–127. [PubMed: 20002199]
39. Mori I, Ohshima Y. Neural regulation of thermotaxis in *Caenorhabditis elegans*. Nature. 1995; 376:344–348. [PubMed: 7630402]
40. Ryu WS, Samuel AD. Thermotaxis in *Caenorhabditis elegans* analyzed by measuring responses to defined thermal stimuli. J Neurosci. 2002; 22:5727–5733. [PubMed: 12097525]
41. Kodama E, Kuhara A, Mohri-Shiomi A, Kimura KD, Okumura M, Tomioka M, Iino Y, Mori I. Insulin-like signaling and the neural circuit for integrative behavior in *C. elegans*. Genes Dev. 2006; 20:2955–2960. [PubMed: 17079685]
42. Mohri A, Kodama E, Kimura KD, Koike M, Mizuno T, Mori I. Genetic control of temperature preference in the nematode *Caenorhabditis elegans*. Genetics. 2005; 169:1437–1450. [PubMed: 15654086]

43. Kuhara A, Mori I. Molecular physiology of the neural circuit for calcineurin-dependent associative learning in *Caenorhabditis elegans*. J Neurosci. 2006; 26:9355–9364. [PubMed: 16971519]
44. Schild LC, Glauser DA. Dynamic switching between escape and avoidance regimes reduces *Caenorhabditis elegans* exposure to noxious heat. Nat Commun. 2013; 4:2198. [PubMed: 23887613]
45. Goodman MB, Klein M, Lasse S, Luo L, Mori I, Samuel A, Sengupta P, Wang D. Thermotaxis navigation behavior; WormBook. 2014. 1–10. www.wormbook.org
46. Benedict FG, Miles WR, Johnson A. The temperature of the human skin. Proc Natl Acad Sci USA. 1919; 5:218–222. [PubMed: 16576376]
47. Burton AC. Human calorimetry: II. The average temperature of the tissues of the body: three figures. J Nutr. 1935; 9:261–280.
48. Castelletto ML, Gang SS, Okubo RP, Tselikova AA, Nolan TJ, Platzer EG, Lok JB, Hallem EA. Diverse host-seeking behaviors of skin-penetrating nematodes. PLoS Pathog. 2014; 10:e1004305. [PubMed: 25121736]
49. Haas W. Parasitic worms: strategies of host finding, recognition and invasion. Zoology. 2003; 106:349–364. [PubMed: 16351919]
50. Bennett NC, Jarvis JUM, Davies KC. Daily and seasonal temperatures in the burrows of African rodent moles. S Afr] Zool. 1988; 23:189–195.
51. Robinson AF. Movement of five nematode species through sand subjected to natural temperature gradient fluctuations. J Nematol. 1994; 26:46–58. [PubMed: 19279868]
52. Ruiz F, Castelletto ML, Gang SS, Hallem EA. Experience-dependent olfactory behaviors of the parasitic nematode *Heligmosomoides polygyrus*. PLoS Pathog. 2017; 13:e1006709. [PubMed: 29190282]
53. Lee J, Dillman AR, Hallem EA. Temperature-dependent changes in the host-seeking behaviors of parasitic nematodes. BMC Biol. 2016; 14:36. [PubMed: 27154502]
54. Monroy FG, Enriquez FJ. *Heligmosomoides polygyrus*: a model for chronic gastrointestinal helminthiasis. Parasitol Today. 1992; 8:49–54. [PubMed: 15463566]
55. Hernandez AD, Sukhdeo MVK. Host grooming and the transmission strategy of *Heligmosomoides polygyrus*. J Parasitol. 1995; 81:865–869. [PubMed: 8544055]
56. Koga M, Nuamtanong S, Dekumyoy P, Yoonuan T, Maipanich W, Rojekittikhun W, Waikagul J. Host-finding behavior of *Strongyloides stercoralis* infective larvae to sodium cation, human serum, and sweat. Southeast Asian J Trop Med Public Health. 2005; 36:93–98. [PubMed: 16438188]
57. Safer D, Brenes M, Dunipace S, Schad G. Urocanic acid is a major chemoattractant for the skin-penetrating parasitic nematode *Strongyloides stercoralis*. Proc Natl Acad Sci USA. 2007; 104:1627–1630. [PubMed: 17234810]
58. McMeniman CJ, Corfas RA, Matthews BJ, Ritchie SA, Vosshall LB. Multimodal integration of carbon dioxide and other sensory cues drives mosquito attraction to humans. Cell. 2014; 156:1060–1071. [PubMed: 24581501]
59. Aoki I, Mori I. Molecular biology of thermosensory transduction in *C. elegans*. Curr Opin Neurobiol. 2015; 34:117–124. [PubMed: 25840145]
60. Glauser DA, Goodman MB. Molecules empowering animals to sense and respond to temperature in changing environments. Curr Opin Neurobiol. 2016; 41:92–98. [PubMed: 27657982]
61. Bargmann CI. Chemosensation in *C. elegans*; WormBook. 2006. 1–29. www.wormbook.org
62. Lok JB. *Strongyloides stercoralis:* a model for translational research on parasitic nematode biology. WormBook. 2007. www.wormbook.org
63. Lok JB, Shao H, Massey HC, Li X. Transgenesis in *Strongyloides* and related parasitic nematodes: historical perspectives, current functional genomic applications and progress towards gene disruption and editing. Parasitology. 2016; 144:327–342. [PubMed: 27000743]
64. Ward JD. Rendering the intractable more tractable: tools from *Caenorhabditis elegans* ripe for import into parasitic nematodes. Genetics. 2015; 201:1279–1294. [PubMed: 26644478]
65. Gang SS, Castelletto ML, Bryant AS, Yang E, Mancuso N, Lopez JB, Pellegrini M, Hallem EA. Targeted mutagenesis in a human-parasitic nematode. PLoS Pathog. 2017; 13:e1006675. [PubMed: 29016680]

66. Diawara A, Schwenkenbecher JM, Kaplan RM, Prichard RK. Molecular and biological diagnostic tests for monitoring benzimidazole resistance in human soil-transmitted helminths. Am J Trop Med Hyg. 2013; 88:1052–1061. [PubMed: 23458960]

67. Keiser J, Utzinger J. Efficacy of current drugs against soil-transmitted helminth infections: systematic review and meta-analysis. JAMA. 2008; 299:1937–1948. [PubMed: 18430913]

68. Kumar N, Rao TK, Varghese A, Rathor VS. Internal parasite management in grazing livestock. J Parasit Dis. 2013; 37:151–157. [PubMed: 24431559]

69. Roeber F, Jex AR, Gasser RB. Impact of gastrointestinal parasitic nematodes of sheep, and the role of advanced molecular tools for exploring epidemiology and drug resistance - an Australian perspective. Parasit Vectors. 2013; 6:153. [PubMed: 23711194]

70. Felippelli G, Lopes WD, Cruz BC, Teixeira WF, Maciel WG, Favero FC, Buzzulini C, Sakamoto C, Soares VE, Gomes LV, et al. Nematode resistance to ivermectin (630 and 700mug/kg) in cattle from the Southeast and South of Brazil. Parasitol Int. 2014; 63:835–840. [PubMed: 25130588]

71. Rund SS, O'Donnell AJ, Gentile JE, Reece SE. Daily rhythms in mosquitoes and their consequences for malaria transmission. Insects. 2016; 7

72. Hunt VL, Tsai IJ, Coghlan A, Reid AJ, Holroyd N, Foth BJ, Tracey A, Cotton JA, Stanley EJ, Beasley H, et al. The genomic basis of parasitism in the *Strongyloides* clade of nematodes. Nat Genet. 2016; 48:299–307. [PubMed: 26829753]

73. Howe KL, Bolt BJ, Cain S, Chan J, Chen WJ, Davis P, Done J, Down T, Gao S, Grove C, et al. WormBase 2016: expanding to enable helminth genomic research. Nucleic Acids Res. 2016; 44:D774–780. [PubMed: 26578572]

74. Junio AB, Li X, Massey HC Jr, Nolan TJ, Todd Lamitina S, Sundaram MV, Lok JB. *Strongyloides stercoralis*: cell- and tissue-specific transgene expression and co-transformation with vector constructs incorporating a common multifunctional 3' UTR. Exp Parasitol. 2008; 118:253–265. [PubMed: 17945217]

75. Hawdon JM, Schad GA. Long-term storage of hookworm infective larvae in buffered saline solution maintains larval responsiveness to host signals. J Helm Soc Wash. 1991; 58:140–142.

76. White GF. A method for obtaining infective nematode larvae from cultures. Science. 1927; 66:302–303.

77. Stiernagle T. Maintenance of *C. elegans*; WormBook. 2006. 1–11. www.wormbook.org

78. Karp X. Working with dauer larvae; WormBook. 2016. 1–19. www.wormbook.org

79. Schindelin J, Arganda-Carreras I, Frise E, Kaynig V, Longair M, Pietzsch T, Preibisch S, Rueden C, Saalfeld S, Schmid B, et al. Fiji: an open-source platform for biological-image analysis. Nat Methods. 2012; 9:676–682. [PubMed: 22743772]

80. Kearse M, Moir R, Wilson A, Stones-Havas S, Cheung M, Sturrock S, Buxton S, Cooper A, Markowitz S, Duran C, et al. Geneious Basic: an integrated and extendable desktop software platform for the organization and analysis of sequence data. Bioinformatics. 2012; 28:1647–1649. [PubMed: 22543367]

81. Hammer Ø, Harper DAT, Ryan PD. PAST: Paleontological statistics software package for education and data analysis. Palaeontol Electronica. 2001; 4:9p.

Highlights

- Skin-penetrating human-parasitic nematodes respond robustly to thermal gradients.
- Human-parasitic infective larvae display positive and negative thermotaxis.
- Temperature-driven behaviors can overcome chemical attraction to host odorants.
- Sensory cascades found in free-living nematodes also drive parasite host seeking.

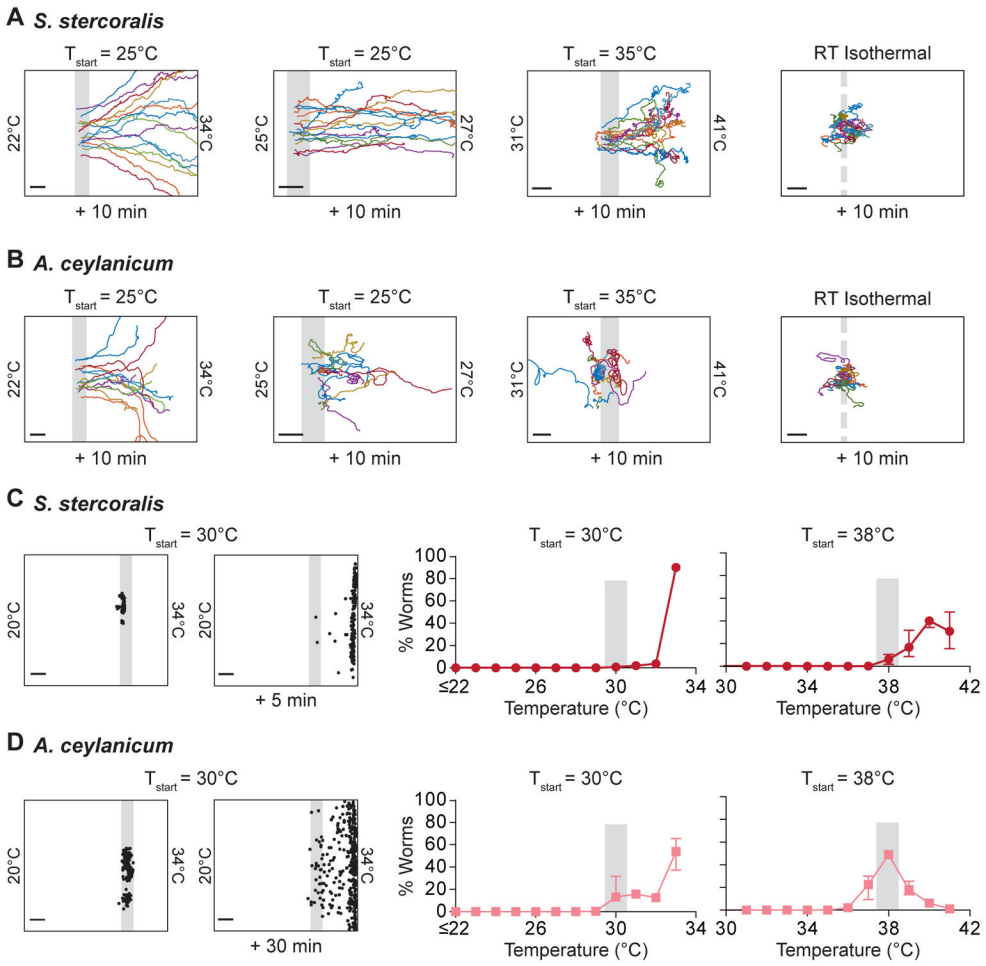

Figure 1. Human-parasitic iL3s show robust heat seeking

(A) Left: Tracks of *S. stercoralis* iL3s heat seeking in a steep thermal gradient (22–34°C, 0.53°C/cm). Starting temperature (T_{start}): ~25°C, duration: 10 min, n=15 worms. Center left: T racks of *S. stercoralis* iL3s heat seeking in a shallow thermal gradient (24–27°C, 0.13°C/cm). T_{start}: ~25°C, duration: 10 min, n=15 worms. Only a portion of the plate (25–27°C) is shown. Center right: Tracks of *S. stercoralis* iL3s moving in a 29–41°C gradient (0.53°C/cm). T_{start}: ~35°C, duration: 10 min, n=15 worms. Only a portion of the gradient (31–41°C) is shown. Right: Tracks of *S. stercoralis* iL3s migrating on an isothermal room temperature (RT) plate. Duration: 10 min, n=15 worms. Tracks reflect movement patterns in the absence of applied sensory stimulation. For each gradient, tracked worms were selected at random from ≤100 iL3s placed on the plates. **(B)** Left: Tracks of *A. ceylanicum* iL3s heat seeking in a steep thermal gradient (22–34°C, 0.53° C/cm). Starting temperature (T_{start}): ~25°C, duration: 10 min, n=15 worms. Center left: Tracks of *A. ceylanicum* iL3s heat seeking in a shallow thermal gradient (24–27°C, 0.13°C/cm). T_{start}: ~25°C, duration: 10 min, n=15 worms. Only a portion of the plate (25–27°C) is shown. Center right: Tracks of *A. ceylanicum* iL3s moving in a 31–42°C gradient (0.49°C/cm). T_{start}: ~35°C, duration: 10 min, n=15 worms. Only a portion of the gradient (31–41°C) is shown. Right: Tracks of *A. ceylanicum* iL3s migrating on an isothermal room temperature (RT) plate. Duration: 10 min,

n=20 worms. For each gradient, tracked worms were selected at random from ≤100 iL3s placed on the plates. **(C)** Left: Representative distribution of *S. stercoralis* iL3s placed at 30°C in a 20–34°C gradient, either a t the start of the experiment or 5 minutes later. Black dots indicate locations of individual iL3s (dots are not to scale). Center: Median final distribution of *S. stercoralis* iL3s in a ~20–34°C gradient (T_{start}: ~30°C, duration: 5 min, n=16 trials with >50 iL3s per trial). Right: Median final distribution of *S. stercoralis* iL3s in a 30–42°C gradient (T_{start}: 38°C, duration: 15 min, n=17 trials with >50 iL3s per trial). Graphs show medians and interquartile ranges; in some cases, error bars are too small to be visible. See also Video S1. **(D)** Left: Representative distribution of *A. ceylanicum* iL3s placed at 30°C in a 20–34°C gradient, either a t the start of the experiment or 30 minutes later. Black dots indicate locations of individual iL3s (dots are not to scale). Center: Median final distribution of *A. ceylanicum* iL3s in a ~20–34°C gradient (T_{start}: ~30°C, duration: 30 min, n=16 trials with >50 iL3s per trial). Right: Median final distribution of *A. ceylanicum* iL3s in a 30–42°C gradient (T_{start}: 38°C, duration: 15 min, n=15 trials with >50 iL3s per trial). Graphs show medians and interquartile ranges; in some cases, error bars are too small to be visible. For all experiments, cultivation temperature (T_C): 23°C, scale bars: 2 cm, grey bars indicate T_{start}, and the width of the grey bars represents 1°C (except f or shallow gradient tracks, where the width of the grey bars represents 0.25°C, and isothermal tracks, where the dashed grey bar indicates approximate starting location of the iL3s). See also Figures S1-S3 and Video S1.

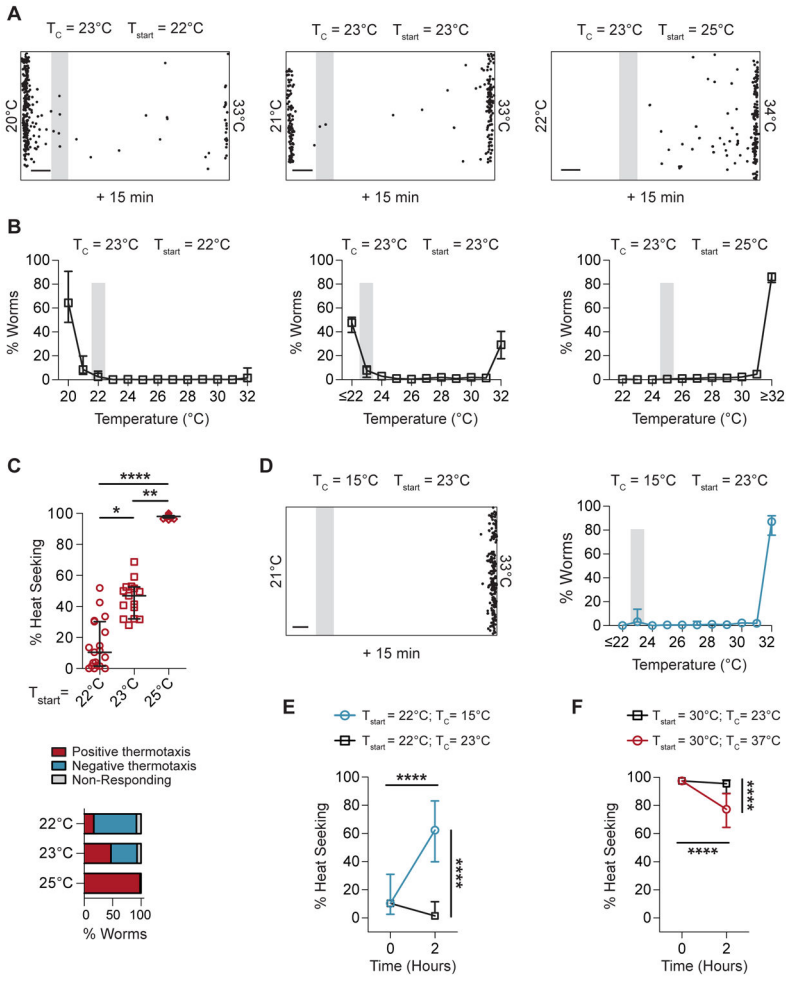

Figure 2. Experience-dependent plasticity regulates a switch between positive and negative thermotaxis

(A) Left: Representative distribution of *S. stercoralis* iL3s placed at 22°C in a 20–33°C gradient after 15 minutes. iL3s display primarily negative thermotaxis. Center: Representative distribution of *S. stercoralis* iL3s placed at 23°C in a 21–33° gradient after 15 minutes. iL3s display both positive and negative thermotaxis. Right: Representative distribution of *S. stercoralis* iL3s placed at 25°C in a 22–34°C gradient after 15 min. iL3s display primarily positive thermotaxis. T_C: 23°C, scale bars: 2 cm, grey bars indicate T_{start}, width of the grey bars represents 1°C. Black dots indicate locations of individual iL3s (dots are not to scale). **(B)** Left: Median final distribution of *S. stercoralis* iL3s placed at 22°C in a 20–33°C gradient. T_C: 23°C, duration: 15 min, n=19 trials with >50 iL3s per trial. Center: Median final distribution of *S. stercoralis* iL3s placed at 23°C in a ~22–33°C gradient. T_C = 23°C; duration: 15 min, n=15 trials with >50 iL3s per trial. Right: Median final distribution of *S. stercoralis* iL3s placed at 25°C in a ~22–33°C gradient. T_C = 23°C, duration: 15 min, scale bars: 2 cm, grey bars indicate T_{start}, width of the grey bars represents 1°C, n=15 trials with >50 iL3s per trial. Graphs show medians and interquartile ranges. In some cases, error bars are too small to be visible. **(C)** Top: Percent of heat-seeking (*i.e.*, positively thermotaxing) *S. stercoralis* iL3s in a ~21–34°C gradient, by starting temperature. *p<0.05,

p<0.005, ****p<0.0001, Kruskal-Wallis test with Dunn's post-test. n=15–19 trials per condition, with >50 iL3s per trial. Bottom: Proportion of *S. stercoralis* iL3s placed at different starting temperatures that display positive or negative thermotaxis, or that fail to migrate out of the initial 1°C temperature bin (non-responding). The percentage of iL3s that engage in thermotaxis (either positive or negative) is not significantly different when iL3s are placed at 22°C versus 23°C (p = 0.45, chi-squared test). However, each increase in starting temperature results in a significant increase in the likelihood of positive thermotaxis (22°C vs 23°C: p<0.001; 23°C vs 25°C: p<0.001; 22°C vs 25°C: p<0.001, chi-squared test with Bonferroni correction). Data are from the experiments shown in B. **(D) Left: Representative distribution of *S. stercoralis* iL3s cultivated at 15°C for 7 days and then placed at 23°C in a 21–33°C gradient. iL3s display only heat seeking. Black dots indicate locations of individual iL3s (dots are not to scale). Right: Median final distribution of *S. stercoralis* iL3s cultivated at 15°C for 7 days and then placed at 23°C in a ~22–33°C gradient. Duration: 15 min, n=15 trials with >50 iL3s per trial. Graph shows medians and interquartile ranges. In some cases, error bars are too small to be visible. **(E)** Time course of the T_C-dependent shift in thermal preference at temperatures below host body temperature (T_H). iL3s were initially cultured at 23°C, and either shifted to 15°C (blue) or maintained at 23°C (black) for 2 hours. The iL3s were then placed at 22°C in a 20–33°C gradient. iL3s that had been cultured at 15°C for 2 hours showed an increased frequency of heat seeking. ****p<0.0001, two-way ANOVA with Tukey's post-test. Duration: 15 min, n=14–15 trials per time point with >50 iL3s per trial. Graph shows medians and interquartile ranges. See also Videos S2 and S3. **(F)** Time course of the T_C-dependent shift in thermal preference at temperatures near T_H. iL3s were initially cultured at 23°C, and then either shifted to 37°C (red) or maintained at 23°C (black) for 2 hours. The iL3s were then placed at 30°C in a 21–33°C gradient. iL3s that had been cultured at 37°C for 2 hours showed a slightly decreased frequency of heat seeking. ****p<0.0001, two-way ANOVA with Tukey's post-test. Duration: 15 min, n=14–15 trials per time point with >50 iL3s per trial. Graph shows medians and interquartile ranges. In some cases, error bars are too small to be visible. See also Figure S4, and Videos S2 and S3.

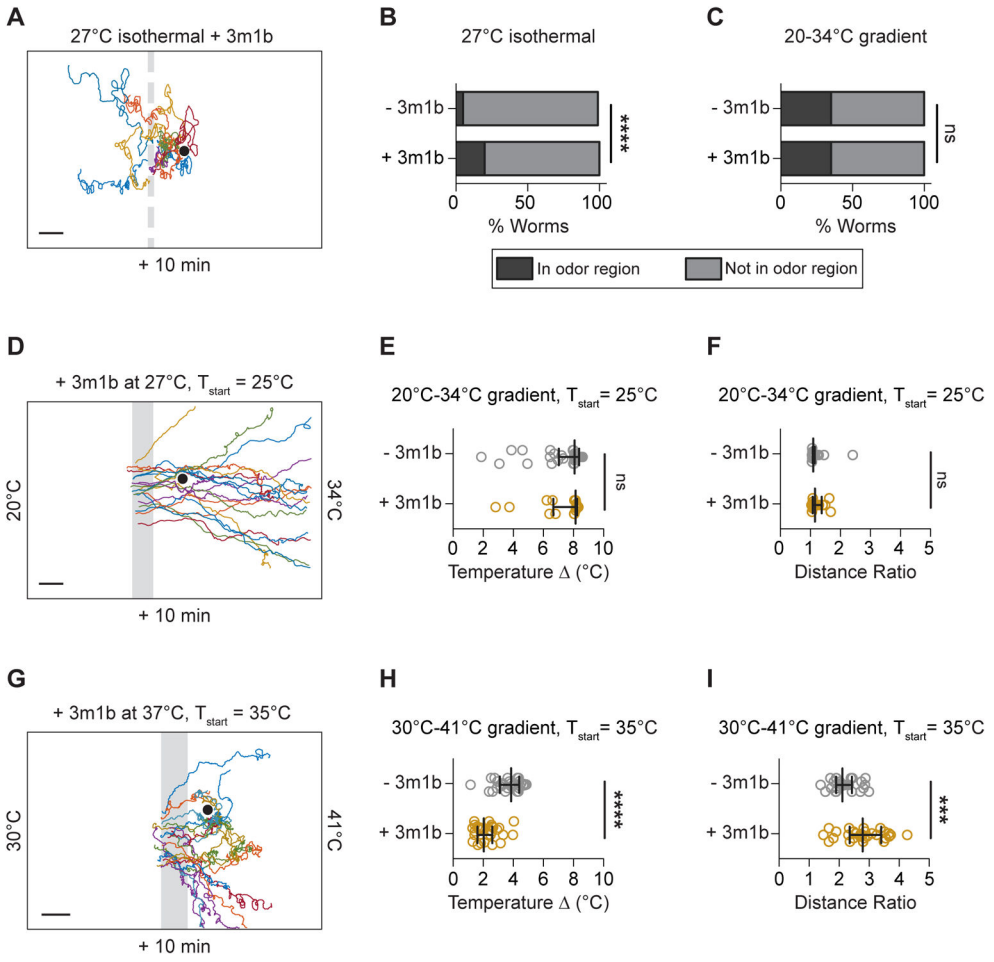

Figure 3. Thermal gradients can override olfactory attraction

(A) *S. stercoralis* iL3 tracks on a 27°C isothermal plate; iL3s divert toward the attractive host odorant 3-methyl-1-butanol (3m1b, 5 μL undiluted) placed ~2 cm away. T_C: 23°C, duration: 10 min, n=10 worms. Dashed bar indicates approximate starting location of iL3s. Scale bar: 2 cm. Tracked worms were selected at random from ≤100 iL3s placed on the plate. **(B)** Percentage of *S. stercoralis* iL3s placed on a 27°C isothermal plate with or without 3 m1b that either entered or failed to enter a 2-cm-diameter scoring region in 5 minutes. The scoring regions were positioned such that on plates with 3m1b, the 3m1b was centered in the scoring region. In an isothermal environment, the presence of 3m1b significantly increased the likelihood that worms entered the scoring region (****p<0.0001, chi-squared test). T_C: 23°C, n=723–760 iL3s across 5 trials per condition. **(C)** Percentage of *S. stercoralis* iL3s placed in a 20–34°C gradient with or without 3 m1b that either entered or failed to enter a 2-cm-diameter scoring region in 5 minutes. The scoring regions were positioned such that on plates with 3m1b, the 3m1b was centered in the scoring region. In the thermal gradient, the presence of 3m1b did not alter the percentage of worms entering the scoring region. T_{start}: ~25°C, $T_{odorant}$: 27°C, T_C: 23°C, n=921–924 iL3s across 5 trials per condition. ns=not significant, chi-squared test. **(D)** *S. stercoralis* iL3 tracks in a 20–34°C gradient with 3m1b placed at 27°C. T_{start}: ~25°C, $T_{odorant}$: 27°C, T_C: 23°C, duration: 10 min, n=20 worms. Scale bar: 2 cm. Tracked worms were selected at random from ≤100 iL3s placed on the

plate. **(E)** The presence of 3m1b placed at 27°C in a 20–34°C gradient does not alter the final temperature reached by iL3s migrating in the gradient. Graph shows the change in temperature (final temperature - starting temperature) exhibited by individual iL3s migrating in a 20–34°C thermal gradient versus a combined 20–34°C thermal/ chemosensory gradient. T_{start}: ~25°C, $T_{odorant}$: 27°C, T_C: 23°C, duration: 10 min, n = 20–40 iL3s per condition. ns = not significant, Mann-Whitney test. Lines show medians and interquartile ranges. **(F)** The presence of 3m1b placed at 27°C in a 20–34°C gradient does not alter the tortuosity of *S. stercoralis* iL3 movement paths. Graph shows the distance ratios of individual iL3s migrating in a 20–34°C thermal gradient versus a combined 20–34°C thermal/chemosensory gradient. Distance ratios were calculated as the total track length divided by the maximum displacement; a higher value indicates a more highly curved trajectory. T_{start}: ~25°C, $T_{odorant}$: 27°C, T_C: 23°C, duration: 10 min, n = 20–40 worms per condition. ns = not significant, Mann-Whitney test. Lines show medians and interquartile ranges. **(G)***S. stercoralis* iL3 tracks in a 29–41°C gradient with 3m1b placed at 37°C. T_{start}: ~35°C, $T_{odorant}$: 37°C, T_C: 23°C, duration: 10 min, n=20 worms. Scale bar: ~2 cm. Only a portion of the plate (30–41°C) is shown. Tracked worms were selected at random from ≤100 iL3s placed on the plate. **(H)** The presence of 3m1b placed at 37°C in a 29–41°C gradient decreases the final temperature reached by iL3s migrating in the gradient. Graph shows the change in temperature (final temperature - starting temperature) exhibited by individual iL3s migrating in a 29–41°C thermal gradient versus a combined 29–41°C thermal/chemosensory gradient. T_{start}: ~35°C, $T_{odorant}$: 37°C, T_C: 23°C, duration: 10 min, n = 30 worms per condition. ****p<0.0001, Mann-Whitney test. Lines show medians and interquartile ranges. **(I)** The presence of 3m1b placed at 37°C in a 29–41°C gradient increases the tortuosity of *S. stercoralis* iL3s movement paths. Graph shows the distance ratios of individual iL3s migrating in a 29–41°C thermal gradient versus a combined 29–41°C thermal/ chemosensory gradient, calculated as described in F. T_{start}: ~35°C, $T_{odorant}$: 37°C, T_C: 23°C, duration: 10 min, n = 30 worms per condition. ***p<0.0005, Mann-Whitney test. Lines show medians and interquartile ranges.

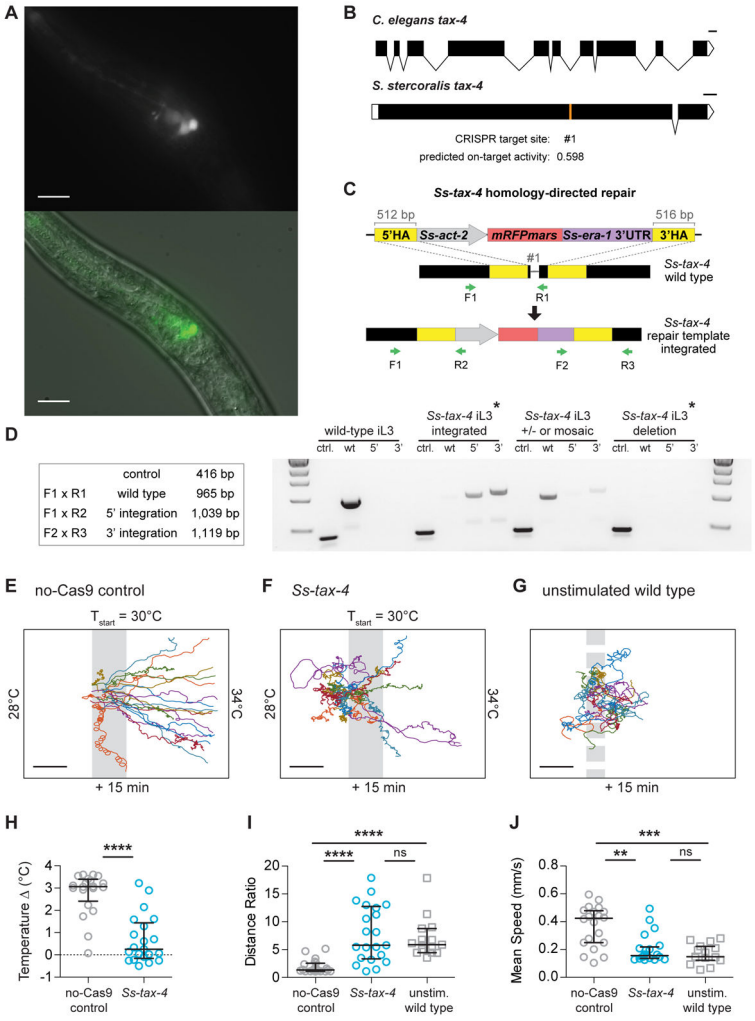

Figure 4. The *S. stercoralis tax-4* homolog is required for heat seeking

(A) *Strongyloides-tax-4p::GFP* is expressed in the head neurons of an *S. stercoralis* larva. Scale bar: 10 μM. **(B)** The *tax-4* genes of *C. elegans* and *S. stercoralis.* The *Ss-tax-4* gene structure was based on the gene prediction by WormBase Parasite [65, 72, 73]. The location of the CRISPR target site is marked, and the on-target activity score is indicated. Scale bars = 100 base pairs. **(C)** Strategy for homology-directed repair and single-worm genotyping at the *Ss-tax-4* target site [65]. The repair template contains an *mRFPmars* reporter gene under the control of the *Ss-act-2* promoter, which expresses in body wall muscle [74]. Free-living adult females (P_0) were microinjected with plasmids containing the CRISPR components (*Cas9*, single guide RNA, and repair template). F_1 iL3 progeny with near-uniform *Ss-act2p::mRFPmars* expression throughout the body wall were then genotyped using the primer sets indicated (green arrows). The wild- type primer set (F1/R1) exclusively amplifies the wild-type locus surrounding the *Ss-tax-4* target site. The 5' and 3' integration primers (F1/R2 and F2/R3, respectively) only amplify following successful integration of the repair template containing *Ss-act2::mRFPmars* at the *Ss-tax-4* target site. **(D)** Representative genotypes of a wild-type iL3 and F_1 iL3s expressing *mRFPmars* from P_0 females microinjected with the *Ss-tax-4* CRISPR components. ctrl. = control reaction amplifying the

first exon of the *Ss-act-2* gene to confirm the presence of genomic DNA; wt = reaction for the wild-type locus; 5' = reaction for insertion of the 5' border of the repair template; 3' = reaction for insertion of the 3' border of the repair template. Asterisks indicate genotypes categorized as *Ss-tax-4* homozygous knockouts. "+/− or mosaic" indicates iL3s that are either heterozygous or mosaic for an *Ss-tax-4* gene disruption [65]. Size markers, from top to bottom: 3 kilobases (kb), 2 kb, 1.5 kb, 1 kb, and 500 base pairs. **(E–F)** CRISPR-Cas9 targeting of the *Ss-tax-4* gene results in iL3s with reduced preferences for warm temperatures. Tracks of individual no-Cas9 control F_1 iL3s (E) and *Ss-tax-4* F_1 iL3s (F) migrating for 15 min in a ~22–34°C gradient (T_{start}: ~30°C, T_C: 23°C; only a portion of the full gradient is show n). Worms were categorized as *Ss-tax-4* homozygous knockouts ("*Ss-tax-4*") if the wild-type *Ss-tax-4* amplification band was absent during *post-hoc* single-worm genotyping. Grey bars: T_{start}, grey bar width: 1°C. Scale bars: ~2 cm. **(G)** Tracks of individual wild-type iL3s migrating for 15 min on an isothermal room temperature (RT) plate; tracks reflect unstimulated movement patterns. Dashed bar indicates approximate starting location of iL3s. T_C: 23°C. Scale bar: 2 cm. Tracked worms were selected at random from ≤100 iL3s placed on the plate. The first 10 min of these tracks are also shown in Figure 1A and quantified in Figure S2. **(H)** Change in temperature (final temperature - starting temperature) exhibited by individual iL3s migrating in a ~22–34°C gradient (T_{start}: ~30°C, T_C: 23°C). No-cas9 control iL3s migrated father up the thermal gradient than *Ss-tax-4* iL3s. ****p<0.0001, Mann-Whitney test. **(I)** Distance ratio (maximum displacement divided by total distance traveled) for no-Cas9 control, *Ss-tax-4*, and unstimulated wild-type iL3s. The presence of the thermal gradient did not suppress local search in *Ss-tax-4* iL3s. ****p<0.0001, Kruskal-Wallis test with Dunn's post-test. ns=not significant. For no-Ca9 control and *Ss-tax-4* iL3s, thermal gradient: 22–34°C gradient, T_{start}: ~30°C, T_C: 23°C. Unstimulated worms were placed on an isothermal room temperature plate, T_C: 23°C. **(J)** Mean speed of iL3s during thermotaxis navigation. *S. stercoralis* iL3s increased their crawling speed at warmer temperatures (no-Cas9 control versus unstimulated wild type), as previously reported [48]. Disruption of *Ss-tax-4* prevented temperature-dependent speed changes. **p<0.005, ***p<0.001, Kruskal-Wallis test with Dunn's post-test. ns=not significant. For no-Ca9 control and *Ss-tax-4* iL3s, thermal gradient: 22–34°C gradient, T_{start}: ~30°C, T_C: 23°C. Unstimulated worms were placed on an isothermal room temperature plate, T_C: 23°C. For H-J, data are represented as median ± interquartile range. n=15–21 trials per condition.